Pseudomagnetoexcitons in strained graphene bilayers without external magnetic fields

Zhigang Wang,[1] Zhen-Guo Fu,[1,2] Fawei Zheng,[1] and Ping Zhang[1,3,*]

[1]*LCP, Institute of Applied Physics and Computational Mathematics, P.O. Box 8009, Beijing 100088, China*

[2]*SKLSM, Institute of Semiconductors, CAS, P.O. Box 912, Beijing 100083, China*

[3]*Beijing Computational Science Research Center, Beijing 100084, China*

(Received 12 June 2012; revised manuscript received 20 January 2013; published 18 March 2013)

We propose a strained graphene double-layer (SGDL) system for detecting pseudomagnetoexcitons (PME) in the absence of external magnetic fields. The carriers in each graphene layer experience different strong pseudomagnetic fields (PMFs) due to strain engineering, which give rise to Landau quantization. The pseudo-Landau levels of electron-hole pairs under inhomogeneous PMFs in the SGDL are obtained analytically in the absence of Coulomb interactions. Based on the derived optical absorption selection rule for PMEs, we interpret the optical absorption spectra as indicating the formation of Dirac-type PMEs. We also predict that in the presence of inhomogeneous PMFs, the superfluidity-normal phase-transition temperature of PMEs is greater than that under homogeneous PMFs.

DOI: 10.1103/PhysRevB.87.125418 PACS number(s): 73.21.Ac, 71.35.Ji, 73.30.+y, 81.05.ue

I. INTRODUCTION

Graphene provides an ideal setting for studying exotic phenomena in condensed-matter physics[1–3] because the charge carriers there behave like massless Dirac particles. Much effort has been devoted to displaying the striking electronic features of graphene, such as the Klein paradox,[4] the anomalous quantum-Hall effect,[5] and others.[2,3] However, it was realized early on that the structural and mechanical properties are important both for theoretical understanding and for applications of graphene,[6] e.g., for strain engineering.[7–14] It was shown recently that specific forms of strain produce a strong pseudomagnetic field (PMF) in graphene,[15] which effectively breaks the time-reversal symmetry.[9] The strain-induced PMF is expected to produce pseudo-Landau level (PLLs) and, consequently, the quantum-Hall effect, even in the absence of an external magnetic field.[10] These intriguing properties extend to graphene multilayers. Recently, the shear mode in graphene multilayers was observed by Raman spectroscopy,[16] and high-temperature Bose-Einstein condensation and superfluidity of indirect excitons or electron-hole pairs in graphene n-p bilayers[17–20] are also predicted. In contrast to other bilayer n-p systems, such as coupled semiconductor quantum wells,[21–23] n-p-type strained graphene double layers (SGDLs) separated by a dielectric layer should be an ideal system for creating pseudomagnetoexcitons (PMEs) due to the PMF induced by strain, rather than to an applied magnetic field. Because of the difference of ripples or elastic deformations in each graphene layer sample on a substrate, it is in fact more realistic to fabricate different or inhomogeneous PMFs in electron and hole layers, which is difficult to achieve with external magnetic fields.

On the basis of these interesting and plausible hypotheses, we herein theoretically analyze the properties of these PMEs in a SGDL system in the absence of a magnetic field. Below, we show that the formation of PMEs in a SGDL can be determined from the optical absorption selection rule of PMEs, which is related to the imbalance parameter $\gamma = \sqrt{B_s^h/B_s^e}$ of the strain-induced PMFs B_s^h and B_s^e experienced by Dirac holes and electrons in a SGDL. We also find by comparison with the homogeneous case ($\gamma = 1$) that the critical temperature of the Kosterlitz-Thouless (KT) transition is improved by a factor of $[(2+\gamma+\gamma^{-1})/4]^2$ in the inhomogeneous case. We also suggest some useful technical tips for designing the SGDL setup for detecting PMEs.

Our system, illustrated in Fig. 1, consists of two parallel strained graphene layers separated by an insulating slab of SiO_2. By varying the chemical potential by tuning the bias voltages of the two gates located near the corresponding graphene sheets, spatially separated electrons and holes can be generated in the different layers. To obtain the analytical PLL expression, we assume that both graphene sheets are bent into cylindrical arcs,[11] which can give rise to PMFs $B_s^{e/h} = 8\beta c^{e/h}/a_0$ (in units of $\hbar/e \equiv 1$), and the corresponding fictitious gauge field vector potentials can be chosen as $\boldsymbol{A}_s^{e/h} = B_s^{e/h}(0, x^{e/h})$. Here, $a_0 \approx 1.42$ Å is the lattice constant, $\beta = -\partial \ln t/\partial \ln a_0 \approx 2$, $t \approx 3$ eV denotes the nearest-neighbor hopping parameter, and $c^{e/h}$ is the numerical constant representing the strength of strain in electron/hole layers. In general $c^e \neq c^h$, and therefore $B_s^e \neq B_s^h$ in a SGDL system, which results in the deviation of γ from 1.

II. PME DISPERSION IN SGDL

This SGDL system is described by the Hamiltonian $H = H_0 + U(\boldsymbol{r}^e - \boldsymbol{r}^h)$, where

$$H_0 = \hbar v_f\big[\pi_x^e\sigma_1\otimes\sigma_0 - \pi_y^e\sigma_2\otimes\sigma_0 + \pi_x^h\sigma_0\otimes\sigma_1 - \pi_y^h\sigma_0\otimes\sigma_2\big], \quad (1)$$

with the Fermi velocity $v_f \approx 10^6$ ms^{-1}, $\boldsymbol{\pi}^{e/h} = \boldsymbol{p}^{e/h} \mp \frac{e}{c}\boldsymbol{A}_s^{e/h}$, and the Pauli matrices σ_i ($i = 0,1,2$). $U(\boldsymbol{r}^e - \boldsymbol{r}^h) = -e^2/\epsilon\sqrt{|\boldsymbol{r}^e - \boldsymbol{r}^h|^2 + d^2}$ is the Coulomb interaction (CI) within a spatially separated electron and hole pair, where d is the spacer layer thickness and ϵ ($\sim$4.5 for SiO_2) denotes the dielectric constant of the spacer layer. In the following analysis, the relative CI strength is denoted by $\lambda \equiv (e^2/\epsilon)/(\hbar v_f)$.

Taking the coordinate transformations

$$\boldsymbol{P} = 2\frac{l_e\boldsymbol{p}^e + l_h\boldsymbol{p}^h}{l_e + l_h}, \quad \boldsymbol{p} = \frac{l_e\boldsymbol{p}^e - l_h\boldsymbol{p}^h}{l_e + l_h}, \quad (2)$$

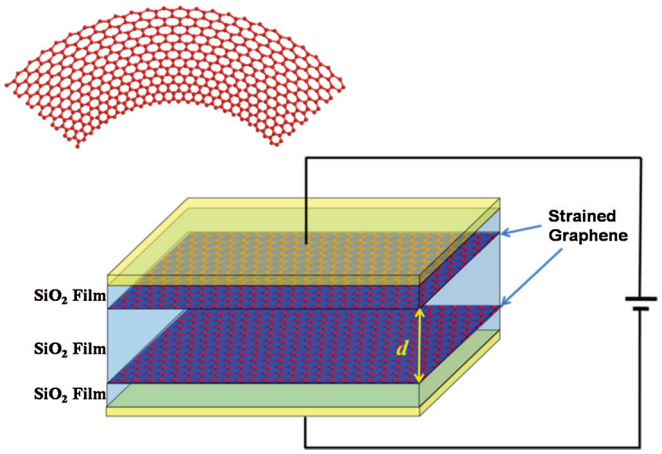

FIG. 1. (Color online) Basic scheme of the proposed SGDL device. Two strained graphene monolayers are separated by a dielectric spacer layer. Electron/hole carriers in each layer are created by $n(p)$-type doping or by applied external gate voltages. Indirect PMEs can be generated by PMFs in the SGDL. A uniform PMF is created perpendicular to the surface cylindrical arc of the strained graphene ribbon.

$$\boldsymbol{R} = \frac{l_h \boldsymbol{r}^e + l_e \boldsymbol{r}^h}{l_e + l_h}, \quad \boldsymbol{r} = 2\frac{l_h \boldsymbol{r}^e - l_e \boldsymbol{r}^h}{l_e + l_h}, \tag{3}$$

where $l_{e/h} = \sqrt{\hbar/eB_s^{e/h}}$ ($\sim 26\ \text{nm}/\sqrt{B_s^{e/h}[\text{T}]}$) represents the pseudomagnetic lengths in the electron/hole layer (we later adopt a length unit of $\sqrt{l_e l_h}$), we can rewrite $h_0^{e/h}$ in Eq. (1) as

$$h_0^{e/h} = \left\{\kappa_{e/h}\left(\frac{P_x}{2} \pm p_x\right) + i\left[\left(\frac{P_y}{2} \pm p_y\right) \mp \xi\left(X \pm \frac{x}{2}\right)\right]\right\}, \tag{4}$$

with $\xi = 1/(2l_e l_h)$ and $\kappa_{e/h} = (l_e + l_h)/(2l_{e/h})$. Here, $\gamma = l_e/l_h = \sqrt{B_s^h/B_s^e}$ describes the inhomogeneity of PMFs experienced by electrons and holes in different layers. In the limit of $\gamma = 1$, the problem of PMEs in SGDL is reduced to be consistent with that of the magnetoexcitons in a uniform external magnetic field.[17,24] For further derivations, we introduce a transformation $S = e^{iXy/l_e l_h}$, from which $S^\dagger P_x S = P_x + y/l_e l_h$, $S^\dagger p_y S = p_y + X/l_e l_h$, and $\boldsymbol{r} \to \boldsymbol{r} - l_e l_h \hat{\boldsymbol{z}} \times \boldsymbol{P}$. Subsequently, $h_0^{e/h}$ can be rewritten as

$$h_0^{e/h} = \kappa_{e/h}\{(\pm p_x + \xi y) \pm i(p_y \mp \xi x)\}. \tag{5}$$

The electron-hole relative coordinate in the x-y plane $\boldsymbol{r}^e - \boldsymbol{r}^h$ becomes $\tilde{\boldsymbol{r}} = \frac{1}{2}(\gamma - \gamma^{-1})\boldsymbol{R} + \frac{1}{4}(2 + \gamma + \gamma^{-1})(\boldsymbol{r} - l_e l_h \hat{\boldsymbol{z}} \times \boldsymbol{P})$. Finally, we define the harmonic lowering operators

$$a = \sqrt{l_e l_h}\, p_x - i\frac{x}{2\sqrt{l_e l_h}}, \quad b = \sqrt{l_e l_h}\, p_y - i\frac{y}{2\sqrt{l_e l_h}}, \tag{6}$$

and their combinations

$$c_\pm = \pm(a \pm ib)/\sqrt{2}. \tag{7}$$

Substituting them into Eq. (1), the free part of the Hamiltonian H can be rewritten as

$$H_0 = \frac{\hbar v_f (l_e + l_h)}{\sqrt{2}(l_e l_h)^{3/2}} \begin{pmatrix} 0 & l_h c_+ & l_e c_-^\dagger & 0 \\ l_h c_+^\dagger & 0 & 0 & l_e c_-^\dagger \\ l_e c_- & 0 & 0 & l_h c_+ \\ 0 & l_e c_- & l_h c_+^\dagger & 0 \end{pmatrix}. \tag{8}$$

Notice that the basis of H_0 is $(A^{(e)}A^{(h)}, B^{(e)}A^{(h)}, A^{(e)}B^{(h)}, B^{(e)}B^{(h)})$, where A and B are sublattices of graphene and the superscripts e and h denote the electron and hole layers, respectively.

The eigenvalue, i.e., the PLLs of H_0 without the CI, is given by

$$E^{(0)}_{n_+,n_-} = \frac{1}{\sqrt{2}}[s_+\sqrt{|n_+|}(1 + \gamma^{-1}) - s_-\sqrt{|n_-|}(1 + \gamma)] \tag{9}$$

in units of $\hbar v_f/\sqrt{l_e l_h}$ with $s_\pm = \text{sgn}(n_\pm)$, and the corresponding eigenstates of H_0 could be expressed as

$$|n_+,n_-\rangle_0 = 2^\eta \begin{pmatrix} s_+ s_- \Phi_{|n_+|-1,|n_-|-1}(\boldsymbol{r}) \\ s_- \Phi_{|n_+|,|n_-|-1}(\boldsymbol{r}) \\ s_+ \Phi_{|n_+|-1,|n_-|}(\boldsymbol{r}) \\ \Phi_{|n_+|,|n_-|}(\boldsymbol{r}) \end{pmatrix}, \tag{10}$$

where $\eta = \frac{\delta_{n_+,0}+\delta_{n_-,0}-2}{2}$, $s_\pm = \text{sgn}(n_\pm)$, and $\Phi_{n_1,n_2}(\boldsymbol{r}) = \frac{2^{-\frac{|l_z|}{2}} n_-! e^{-il_z\phi}\delta(l_z) r^{|l_z|}}{\sqrt{2\pi n_1! n_2!}} L_{n_-}^{|l_z|}(\frac{r^2}{2}) e^{-\frac{r^2}{4}}$, with $l_z = n_1 - n_2$, $n_- = \min(n_1,n_2)$, $\delta(l_z) = \text{sgn}(l_z)^{l_z} \to 1$ for $l_z = 0$, and $L(x)$ being the Laguerre polynomial.

Consider a PME formed by an electron on the Landau level (LL) n and a hole on the LL m. In the limit of the relatively large separation d and high PMF B, namely, when $e^2/(\epsilon\sqrt{r^2 + d^2}) \ll \hbar v_f/\sqrt{l_e l_h}$, the PME energy can be approximated by only taking its zeroth-order part $E^{(0)}_{n,m}$. However, at higher PMF, 10–20 T in experiment, the CI $e^2/(\epsilon\sqrt{r^2 + d^2})$ is only several times less than the zeroth energy $\hbar v_f/\sqrt{l_e l_h}$. In this case, the CI can be treated as a perturbation and divided into an intra-LL part and an inter-LL part. To obtain the eigenvalues E_{n_+,n_-} of the total Hamiltonian H, the CI part U is treated as a perturbation by solving the equation

$$\det\left\|\delta_{n_+,n'_+}\delta_{n_-,n'_-}\left(E^{(0)}_{n_+,n_-} - E\right) + {}_0\langle n'_+,n'_-|U(\tilde{\boldsymbol{r}})|n_+,n_-\rangle_0\right\| = 0 \tag{11}$$

to first order in ${}_0\langle n'_+,n'_-|U|n_+,n_-\rangle_0$, where the intra-PLL component of the CI is defined as ${}_0\langle n_+,n_-|U|n_+,n_-\rangle_0$, while the inter-PLL component is defined as ${}_0\langle n'_+,n'_-|U|n_+,n_-\rangle_0$ with $|n'_+,n'_-\rangle_0 \neq |n_+,n_-\rangle_0$. For the intra-LL part, which dominates the CI, the magnetoexciton energy can be explicitly written as

$$\begin{aligned} E_{n,m} &= E^{(0)}_{n,m} + \langle\Psi_{n,m}|U(\tilde{\boldsymbol{r}})|\Psi_{n,m}\rangle \\ &= E^{(0)}_{n,m} + 2^{\delta_{n,0}+\delta_{m,0}-2} \\ &\quad \times \{\langle\langle|n|-1,|m|-1|U||n|-1,|m|-1\rangle\rangle \\ &\quad + \langle\langle|n|-1,|m||U||n|-1,|m|\rangle\rangle \\ &\quad + \langle\langle|n|,|m|-1|U||n|,|m|-1\rangle\rangle \\ &\quad + \langle\langle|n|,|m||U||n|,|m|\rangle\rangle\}, \end{aligned} \tag{12}$$

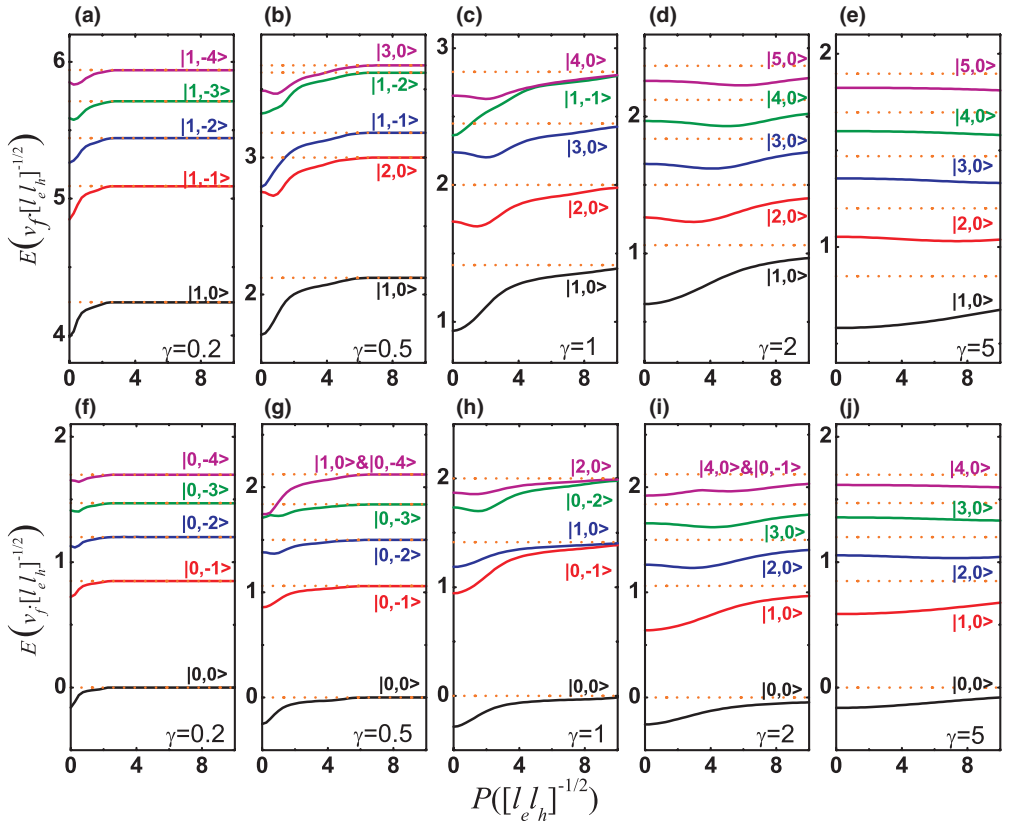

FIG. 2. (Color online) Dispersions of the first few PLLs for (top) the fully occupied case and (bottom) the partially occupied case as functions of P for different γ values. The dashed horizontal lines denote the noninteracting PLLs. The parameters are chosen as $\mu = 0$, $\lambda = 0.49$, $d = 0.2$, and $R = 0$.

where the notation $\langle\langle nm|U|nm\rangle\rangle$ denotes the averaging by the two-dimensional harmonic oscillator eigenfunctions $\Phi_{n,m}(r)$.

The imbalance parameter γ reduces the degeneracy of the PLLs of H_0. For instance, $|1,0\rangle_0$ and $|0,-1\rangle_0$ are degenerate ($E^{(0)}_{1,0} = E^{(0)}_{0,-1}$) when $\gamma = 1$, while these two states turn out to be nondegenerate when $\gamma \neq 1$. The PLLs E_{n_+,n_-} of PMEs are not only dependent on γ but also related to the effective momentum $\boldsymbol{P}$ and coordinate $\boldsymbol{R}$ of the PME center of mass since U is related to $\boldsymbol{P}$ and $\boldsymbol{R}$ after the transformations. The location of the chemical potential determines the electron and hole PLL that can be populated. For convenience, we here use the symbol μ to denote the highest filled PLL and consider two cases: (i) where the electron PLLs with $n_+ > \mu$ are unoccupied and the hole PLLs with $n_- \leqslant \mu$ are fully occupied and (ii) where the electron PLLs with $n_+ > \mu$ are unoccupied and the hole PLLs with $n_- < \mu$ are fully occupied, while the PLL at μ is partially occupied.

The spectra of the five lowest PLLs are plotted as functions of $\boldsymbol{P}$ in Fig. 2, where the solid (dotted) curves denote the PME dispersion in the presence (absence) of the Coulomb interaction. Figures 2(a)–2(e) correspond to the fully occupied cases, and Figs. 2(f)–2(j) correspond to the partially occupied cases. For small $\boldsymbol{P}$, the solid curves clearly depart from the dotted lines and display a particle-hole pair form rather than a density-wave form, whereas with increasing momentum $\boldsymbol{P}$, the PME dispersion relation approaches the noninteracting dispersion relation. Thus, in the present case, Kohn's theorem does not apply, and therefore the energy dispersion and the optical absorption spectrum (see Fig. 4 and the following text) of our PME are different from the conventional (nonrelativistic) two-dimensional electron gas. There, the magnetoexciton energy in the long-wavelength limit is insensitive to electron interactions by virtue of Kohn's theorem.

The PME dispersion also depends strongly on the imbalance parameter γ, as shown in Fig. 2. On the one hand, if the difference in elastic deformation between the electron and hole layers is large (i.e., γ differs significantly from 1), the PME dispersion accelerates the transition from the density-wave form to the particle-hole-pair form with increasing momentum $\boldsymbol{P}$. On the other hand, when γ is not much different from 1, the PME dispersion behaves like that of magnetoexcitons in perfect double-layer graphene in an external magnetic field. Taking the partially occupied cases as an example, we found that, for $\gamma \gg 1$, the lowest PLLs behave like the electron-type state $|n_+,0\rangle$ [see, for example, Fig. 2(j)], while for $\gamma \ll 1$ the lowest PLLs behave like the hole-type state $|0,n_-\rangle$ [Fig. 2(f)].

In contrast to magnetoexcitons in an external magnetic field, the PME dispersion is also related to $\boldsymbol{R}$. By increasing R, the PME dispersion at smaller P acquires a particle-hole-pair form rather than a density-wave form, which can be seen in Fig. 3.

III. OPTICAL ABSORPTION PROPERTIES OF PME IN SGDL

Optical absorption spectroscopy analysis is a useful method for studying magnetoexciton properties because it allows the

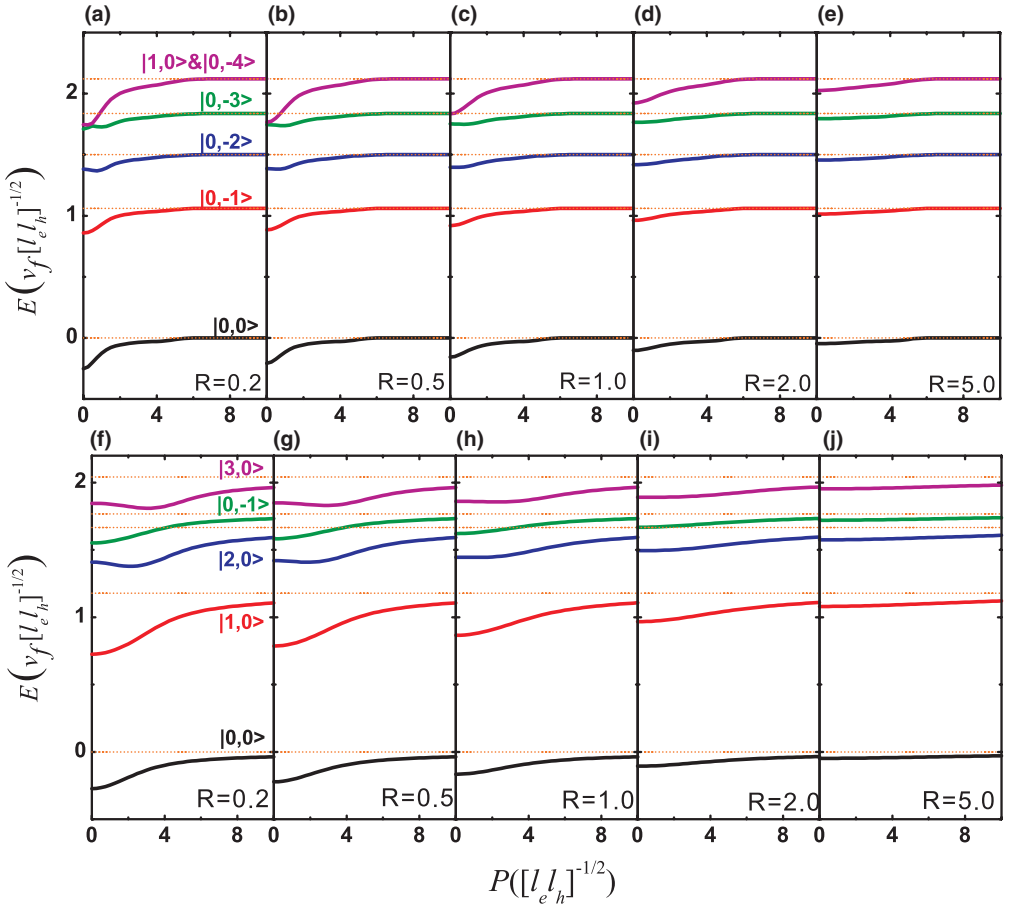

FIG. 3. (Color online) Dispersions of the first few PLLs as functions of P with different R. The imbalance parameter $\gamma = 0.5$ for (a)–(e), while $\gamma = 1.5$ for (f)–(j), and the other parameters are the same as used in Fig. 2.

determination of magnetoexciton energies and wave functions for $\boldsymbol{P} = 0$. The particle-hole excitation energy is obtained directly from the resonant peaks in the magneto-optical absorption spectrum. From Fermi's golden rule, the optical absorption for photons of frequency ω yields

$$R_{ab}(R,\omega) = \frac{2\pi}{\hbar}\sum_{\alpha}\left|\langle\alpha|\frac{e}{c}\boldsymbol{A}\cdot\boldsymbol{v}|0\rangle\right|^2\delta\left(\varepsilon_{eh}^{(\alpha)}(R)-\varepsilon_0-\hbar\omega\right). \tag{13}$$

Here $|\alpha\rangle$ is the set of quantum numbers describing a particle-hole excitation and $|0\rangle \equiv |\mu,\mu\rangle$ is the ground state with energy ε_0 in the absence of a particle-hole excitation. $\boldsymbol{v} = \partial H_0/\hbar\partial\boldsymbol{p}$ is the velocity operator for the free part of the Hamiltonian, and $\boldsymbol{A}$ is the vector potential. For linear polarized light $\boldsymbol{A} = A\hat{\mathbf{x}}$, choosing a Lorentzian-type broadening, one has

$$R_{ab}(R,\omega)\sum_{\alpha}|\langle\alpha|v_x|0\rangle|^2\frac{\Gamma/2}{\left[\varepsilon_{eh}^{(\alpha)}(R)-\varepsilon_0-\hbar\omega\right]^2+\Gamma^2/4}, \tag{14}$$

where Γ denotes the linewidth and $|\langle\alpha|v_x|0\rangle|^2 = \sum_{n_+>\mu}\sum_{n_-\leqslant\mu}\int T d\boldsymbol{r}$ is for full occupation and $\sum_{n_+\geqslant\mu}\sum_{n_-\leqslant\mu}\int T d\boldsymbol{r}$ is for partial occupation. The parameter T is defined as

$$T = \left|C^{\alpha}_{n_+,n_-}\langle n_+,n_-|v_x|\mu,\mu\rangle\right|^2, \tag{15}$$

where $C^{\alpha}_{n_+,n_-}$ is the projection of PME state $|\alpha\rangle$ on the basis state $|n_+,n_-\rangle$.

In the absence of inter-PLL CI, which is much weaker than intra-PLL CI, the PME state $|\alpha\rangle$ is one special basis state, and $C^{\alpha}_{n_+,n_-} = \delta_{\alpha,(n_+,n_-)}$, the same as that in the noninteracting case. Subsequently, the PME optical absorption selection rule for linear polarized light ($\boldsymbol{A} = A\hat{\mathbf{x}}$) is analytically expressed as

$$\begin{aligned}&\langle n_+,n_-|v_x|\mu,\mu\rangle\\ &\quad= c_1\delta_{|n_+|,|\mu|}\delta_{|n_-|,|\mu|-1}+c_2\delta_{|n_+|,|\mu|-1}\delta_{|n_-|,|\mu|}\\ &\qquad+c_3\delta_{|n_+|,|\mu|}\delta_{|n_-|,|\mu|+1}+c_4\delta_{|n_+|,|\mu|+1}\delta_{|n_-|,|\mu|},\end{aligned} \tag{16}$$

where $v_x = \partial H_0/\hbar\partial p_x$ is the velocity operator for the free part of the Hamiltonian and the coefficients $c_1 = -(1+\gamma)s_-(s_\mu s_+ + 1)C$, $c_2 = (1+\gamma^{-1})(s_\mu + s_-)C$, $c_3 = -(1+\gamma)(s_\mu + s_+)C$, and $c_4 = (1+\gamma^{-1})s_+(s_\mu s_- + 1)C$, with $C = v_f(\sqrt{2})^{\delta_{n_+,0}+\delta_{n_-,0}+2\delta_{\mu,0}-6}$. This optical absorption selection rule formula (16) allows a better analysis of the PME absorption resonant peaks in SGDL device spectra. Notice that the optical absorption formula (16) also depends on $\boldsymbol{R}$, as the PME spectrum is related to $\boldsymbol{R}$. As a result, the experimentally observed absorption spectrum is usually an average over different values of R. However, with R deviating from zero, we find that the absorption frequency shifts very little. Therefore, we here only consider the $R = 0$ case.

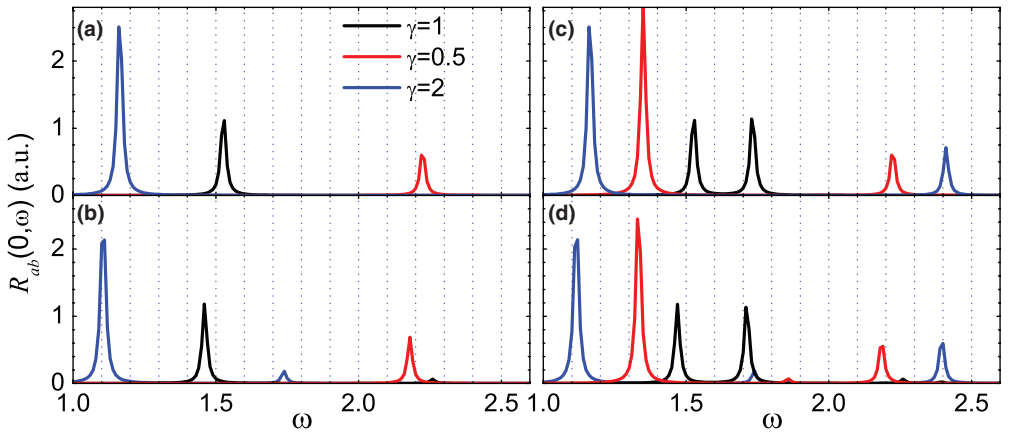

FIG. 4. (Color online) The optical absorption curves for PMEs with $\mu = 0$ for (a) and (b) the fully and (c) and (d) the partially occupied cases, plotted as functions of the photon energy ω ($\hbar = 1$). The inter-PLL CIs are not taken into account in (a) and (c), but they are in (b) and (d). The spacer thickness is set to $d = 0.2$. $\lambda = 0.49$.

In the fully occupied case with $\mu \geqslant 0$, the selection rule can be simplified further as

$$\langle n_+, n_- | v_x | \mu, \mu \rangle = c_4 \delta_{n_+, \mu+1} \delta_{n_-, \mu}, \tag{17}$$

which indicates that there is only one resonance peak in the optical absorption spectrum and which signals PME formation. For example, the selection rule in the fully occupied case of $\mu = 0$ with the ground state $|0,0\rangle$ predicts a single resonance peak, corresponding to the formation of the PME state $|1,0\rangle$ [see Fig. 4(a)]. The red (blue) curve in Fig. 4(a) also clearly shows the shift of the resonance peak toward higher (lower) frequencies as the imbalance parameter γ decreases (increases) from 1.

This effect of inhomogeneity of the PMFs is also apparent for the partially occupied cases, illustrated in Fig. 4(c). According to the general selection rule (16), there are nonzero elements in $\langle n_+, n_- | v_x | 0,0 \rangle$ for only the two PMEs states, $|1,0\rangle$ and $|0,-1\rangle$, giving rise to two resonance peaks in Fig. 4(c). Interestingly, the resonance peak for $|0,-1\rangle$ moves toward lower (higher) frequencies as γ decreases (increases) from 1. In contrast, the resonance peak for $|1,0\rangle$ moves toward higher (lower) frequencies.

We have not yet considered the effect of the inter-PLL CI on PME optical absorption. With the inter-PLL CI included, typical results, shown in Figs. 4(b) and 4(d), are plotted for comparison with Figs. 4(a) and 4(c), respectively. Because the inter-PLL CI mixes the noninteracting PLLs, the absorption phenomenon should appear at the energy of every PME state. This gives rise to new resonance peaks in Figs. 4(b) and 4(d). The magnitudes of these additional resonant peaks are very small, increasingly so as the spacer thickness d increases. Further, the main absorption peaks shift toward lower frequencies. This "redshift" effect can be exploited to study the effect of PLL mixing experimentally. Therefore, based on the optical absorption selection rule analyzed above, optical techniques should allow the detection of PMEs locally as well as the CI effects in the present SGDL device.

The results for cases with $\mu \neq 0$ are similar to those for $\mu = 0$, and an example for $\mu = 1$ is shown in Fig. 5. The selection rule for the fully occupied case with $\mu = 1$ promises that there is only one resonant peak to occur, which corresponds to the formation of PME state $|2,1\rangle$ by absorbing a photon quanta $\hbar\omega$ [see Fig. 5(a)]. For the partially occupied case, however, there are three nonzero elements according to selection rule (17), which are $|1,0\rangle$, $|1,-2\rangle$, and $|2,1\rangle$. Therefore, there are three resonant peaks appearing in the optical absorption spectra; see Fig. 5(c). Similar to those in Fig. 4 in the main text for the $\mu = 0$ cases, the imbalance of strain-induced PMFs changes the location of the resonances. After taking into account the inter-PLL CIs in calculations, additional satellite peaks appear in the optical absorption spectra, and the main peaks move toward the low frequency, as illustrated in Figs. 5(b) and 5(d).

IV. SUPERFLUIDITY OF PME IN SGDL

PMEs are also ideal for exploring Bose-Einstein condensation since they behave as neutral bosons at low densities. Motivated by its importance both from a fundamental perspective and for applications of graphene-based electronics, we now attempt a theoretical evaluation of the effective mass m_{B_s} ($B_s \equiv \sqrt{B_s^e B_s^h}$ herein) and the superfluid-normal state, i.e., the KT transition temperature T_c of PMEs in this SGDL system. In the limit of $d \to \infty$ and $B_s \to \infty$, the PME energy can be approximated by only considering its zeroth-order part $E_{n,m}^{(0)}$. However, if the PMF is about 10–20 T, the CI can be treated as a perturbation because its amplitude is just several times less than $\hbar v_f / \sqrt{l_e l_h}$. In the absence of inter-PLL CI, by substituting the approximate relation[19]

$$\langle\langle nm\,P | U(\tilde{\boldsymbol{r}}) | nm\,P \rangle\rangle = \varepsilon_{nm}^{(b)} + \frac{P^2}{2M_{mn}(B_s, d)} \tag{18}$$

for $R = 0$ into Eq. (12), we can get the asymptotic dispersion law of the PMEs for small momentum $\boldsymbol{P}$. Here the notation $\langle\langle nm\,P | U(\tilde{\boldsymbol{r}}) | nm\,P \rangle\rangle$ denotes the averaging by the two-dimensional harmonic oscillator eigenfunctions $\Phi_{n,m}(\boldsymbol{r})$, and $\varepsilon_{nm}^{(b)}$ is the binding energy.

As an example, let us consider the case of PMEs on the (1,1) PLL with the small-$\boldsymbol{P}$ energy given by $E_{1,1}(P) = \varepsilon_{B_s}^{(b)}(d) + \frac{P^2}{2m_{B_s}(d)}$. In the limit $d \gg \sqrt{l_e l_h}$, one can explicitly obtain $\varepsilon_{B_s}^{(b)} = -\frac{e^2}{\epsilon d}$, the same value as for magnetoexcitons in

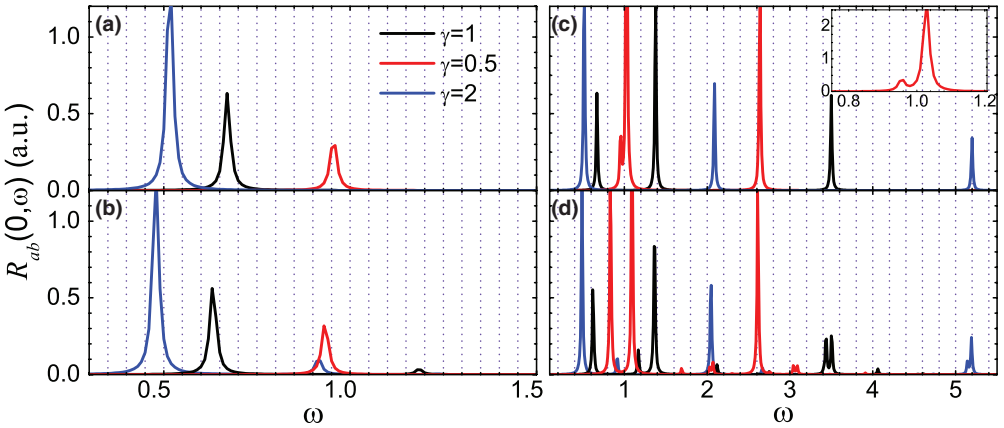

FIG. 5. (Color online) The optical absorption curves of PMEs with $\mu = 1$. (a) and (b) Fully and (c) and (d) partially occupied cases as functions of photon energy ω ($\hbar = 1$). In (a) and (c) the inter-PLL CIs are not taken into account, while in (b) and (d) the inter-PLL CIs are taken into account. The spacer thickness is set to $d = 0.2$. $\beta = 0.49$. The inset in (b) is the enlarged dispersion curve between $\omega = 0.8$ and $\omega = 1.2$.

an external magnetic field, since $\varepsilon_{B_s}^{(b)}(d)$ is independent of γ. Whereas the effective mass of a PME should be

$$m_{B_s} = [4/(2+\gamma+\gamma^{-1})]^2 \frac{\epsilon}{4c^2} d^3 B_s^2, \tag{19}$$

where the prefactor $[4/(2+\gamma+\gamma^{-1})]^2$ reduces to unity for homogeneous PMFs (i.e., $\gamma = 1$), the effective mass of the PME in a SGDL is $[4/(2+\gamma+\gamma^{-1})]^2$ times that of magnetoexcitons in perfect double-layer graphene under an external magnetic field. This difference between the effective masses is reflected in the KT transition temperature T_c as follows:

$$T_c = \left[\left(\sqrt{\frac{32}{27}\left[\left(sm_{B_s}k_B T_c^0\right)/(\pi\hbar^2 n)\right]^3 + 1} + 1\right)^{1/3} - \left(\sqrt{\frac{32}{27}\left[\left(sm_{B_s}k_B T_c^0\right)/(\pi\hbar^2 n)\right]^3 + 1} - 1\right)^{1/3}\right] \frac{T_c^0}{2^{1/3}}, \tag{20}$$

where the auxiliary quantity is $T_c^0 = \frac{1}{k_B}\left(\frac{\pi\hbar^2 n \mu_0^2}{6s\zeta(3)m_{B_s}}\right)^{1/3}$, $\mu_0 = \frac{\pi\hbar^2 n}{sm_{B_s}\log[s\hbar^4\epsilon^2/(2\pi n m_{B_s}^2 e^4 d^4)]}$ is the chemical potential of the system, $s = 4$ is the spin degeneracy of PMEs in SGDL, and $\zeta(3)$ is the Riemann zeta function. Here, $n = n_s + n_n$, with n_n being the normal component density and n_s being the superfluid density. Because μ_0 is approximately inversely proportional to the effective mass, the critical temperature of the KT transition of PMEs in SGDL should be greater than that of magnetoexciton in double-layer graphene in an external magnetic field by a factor of the order of $[(2+\gamma+\gamma^{-1})/4]^2$.[19] Typical results of Eq. (20) are shown by the thick curves in Fig. 6. From this, we can conclude that increasing the imbalance of the strains (by making γ sufficiently different from 1) in the different layers of a SGDL device may effectively enhance the KT transition temperature of the PMEs. A large imbalance parameter γ is also realistic since the PMF can be tuned to as high as 300 T in experiments.[15] Because there is no direct bonding interaction between the electron and hole layers in our double-layer system, the PMF in each layer can be tuned independently.

V. EXPERIMENTAL PROPOSAL

To design the required SGDL system in practice, graphene ribbons can first be deposited onto an elastic substrate and then deformed by bending the substrate into a cylindrical arc automatically (Fig. 1). Prior to graphene transfer onto a SiO_2 thin film, graphene layers, prepared by micromechanical cleavage of graphite, are deposited on two different flexible substrates, and then the substrates are deformed by a two-point or four-point bending setup.[25] The strength of strain could be measured by Raman spectroscopy. In order to produce controllable and reproducible strain on slippage, it is extremely important to apply the strain in the most controlled way.[25] This is then transferred onto the SiO_2 thin film[26,27] before carefully removing the elastic substrate by heating or dissolving it with a chemical agent. A uniform PMF can be created in graphene ribbons deposited on SiO_2 thin film since the strain distribution in the substrate projects onto the graphene ribbon. In practice, however, the PMFs produced by strain in the outer and inner bent graphene ribbons may be different because of their different automatic deformations. This justifies our discussion of the importance of the imbalance parameter γ. Metal electrodes are then grown or evaporated on the other side of the SiO_2 thin film, and the device is finally packaged for measurements.

The possibility of achieving high-quality graphene samples[28] and a strong PMF in graphene, together with the

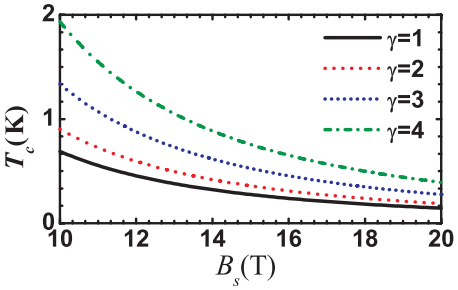

FIG. 6. (Color online) Calculated Kosterlitz-Thouless temperature vs the PMF. The PME density is set to $n = 4.0 \times 10^{11}$ cm^{-2}, and the spacer width $d = 30$ nm.

technical advances in designing graphene multilayer devices, makes it possible to experimentally explore very original optical and superfluidity-normal state KT transition of PMEs in graphene in the absence of an external magnetic field. Moreover, the SGDL system proposed here could also be used to detect the (valley-polarized) unconventional fractional quantum Hall effect of a charged Dirac-type electron-hole fluid or a Bose condensate of PMEs in the absence of an external magnetic field by measuring transport coefficients. Because the fixed number of PMEs corresponds to a fixed valley polarization in the SGDL system, transport studies of the SGDL system will provide unique information that cannot be obtained in direct studies of conventional two-component electron-electron/electron-hole systems.[23]

VI. CONCLUSIONS

In conclusion, we herein proposed a SGDL system, and by considering the relevant physics, we showed this setup can be made to detect PMEs that are associated with elastic deformations or curvature in graphene. The special cases discussed in this paper only served to illustrate the potential for applications of the SGDL system. The fabrication process described above is achievable within currently available experimental techniques. There are at least three differences between PMEs in the SGDL system and the more conventional magnetoexcitons obtained in a real magnetic field: (i) The imbalance of the PMFs in electron and hole layers reduces the PLL degeneracy. (ii) Thus, the PME optical absorption spectrum should be more interesting in the SGDL system. (iii) With increasing strain imbalance between the different layers in SGDL, the KT transition temperature of PMEs will be observably improved. We hope to see these predictions and the suggested SGDL system realized in the near future.

ACKNOWLEDGMENTS

This work was supported by the Natural Science Foundation of China under Grants No. 90921003, No. 10904005, No. 11274049, and No. 11004013 and by the National Basic Research Program of China (973 Program) under Grant No. 2009CB929103.

*Corresponding author: zhang_ping@iapcm.ac.cn

[1] K. S. Novoselov, A. K. Geim, S. V. Morozov, D. Jiang, Y. Zhang, S. V. Dubonos, I. V. Grigorieva, and A. A. Firsov, Science **306**, 666 (2004).

[2] A. H. Castro Neto, F. Guinea, N. M. R. Peres, K. S. Novoselov, and A. K. Geim, Rev. Mod. Phys. **81**, 109 (2009), and references therein.

[3] M. O. Goerbig, Rev. Mod. Phys. **83**, 1193 (2011), and references therein.

[4] M. I. Katsnelson, K. S. Novoselov, and A. K. Geim, Nat. Phys. **2**, 620 (2006).

[5] Y. Zhang, Y.-W. Tan, H. L. Stormer, and P. Kim, Nature (London) **438**, 201 (2005).

[6] A. K. Geim and K. S. Novoselov, Nat. Mater. **6**, 183 (2007).

[7] V. M. Pereira and A. H. Castro Neto, Phys. Rev. Lett. **103**, 046801 (2009).

[8] N. Levy, S. A. Burke, K. L. Meaker, M. Panlasigui, A. Zettl, F. Guinea, A. H. Castro Neto, and M. F. Crommie, Science **329**, 544 (2010).

[9] M. Vozmediano, M. Katsnelson, and F. Guinea, Phys. Rep. **496**, 109 (2010).

[10] F. Guinea, M. I. Katsnelson, and A. K. Geim, Nat. Phys. **6**, 30 (2010).

[11] F. Guinea, A. K. Geim, M. I. Katsnelson, and K. S. Novoselov, Phys. Rev. B **81**, 035408 (2010).

[12] O. Bahat-Treidel, O. Peleg, M. Grobman, N. Shapira, M. Segev, and T. Pereg-Barnea, Phys. Rev. Lett. **104**, 063901 (2010).

[13] F. de Juan, A. Cortijo, M. A. H. Vozmediano, and A. Cano, Nat. Phys. **7**, 810 (2011).

[14] B. Verberck, B. Partoens, F. M. Peeters, and B. Trauzettel, Phys. Rev. B **85**, 125403 (2012).

[15] K. K. Gomes, W. Mar, W. Ko, W. Guinea, and H. C. Manoharan, Nature (London) **483**, 306 (2012).

[16] P. H. Tan, W. P. Han, W. J. Zhao, Z. H. Wu, K. Chang, H. Wang, Y. F. Wang, N. Bonini, N. Marzari, N. Pugno, G. Savini, A. Lombardo, and A. C. Ferrari, Nat. Mater. **11**, 294 (2012).

[17] A. Iyengar, J. H. Wang, H. A. Fertig, and L. Brey, Phys. Rev. B **75**, 125430 (2007).

[18] Y. E. Lozovik and A. A. Sokolik, Pis'ma Zh. Eksp. Teor. Fiz. **87**, 61 (2008) [JETP Lett. **87**, 55 (2008)].

[19] O. L. Berman, Y. E. Lozovik, and G. Gumbs, Phys. Rev. B **77**, 155433 (2008).

[20] O. L. Berman, R. Ya. Kezerashvili, and Y. E. Lozovik, Phys. Rev. B **78**, 035135 (2008).

[21] Y. E. Lozovik and V. I. Yudson, Zh. Eksp. Teor. Fiz. **71**, 738 (1976) [Sov. Phys. JETP **44**, 389 (1976)].

[22] D. W. Snoke, Science **298**, 1368 (2002).

[23] J. P. Eisenstein and A. H. MacDonald, Nature (London) **432**, 691 (2004).

[24] Z. Wang, Z.-G. Fu, and P. Zhang, Appl. Phys. Lett. **100**, 161602 (2012).

[25] T. M. G. Mohiuddin, A. Lombardo, R. R. Nair, A. Bonetti, G. Savini, R. Jalil, N. Bonini, D. M. Basko, C. Galiotis, N. Marzari, K. S. Novoselov, A. K. Geim, and A. C. Ferrari, Phys. Rev. B **79**, 205433 (2009).

[26] S. Roddaro, P. Pingue, V. Piazza, V. Pellegrini, and F. Beltram, Nano Lett. **7**, 2707 (2007).

[27] A. Reina, H. Son, L. Jiao, B. Fan, M. S. Dresselhaus, Z. Liu, and J. Kong, J. Phys. Chem. C **112**, 17741 (2008).

[28] C. Berger, Z.-M. Song, X.-B. Li, X.-S. Wu, N. Brown, C. Naud, D. Mayo, T.-B. Li, J. Hass, A. N. Marchenkov, E. H. Conrad, P. N. First, and W. A. de Heer, Scinece **312**, 1191 (2006).